Belt/zone circulation of giant planet atmospheres

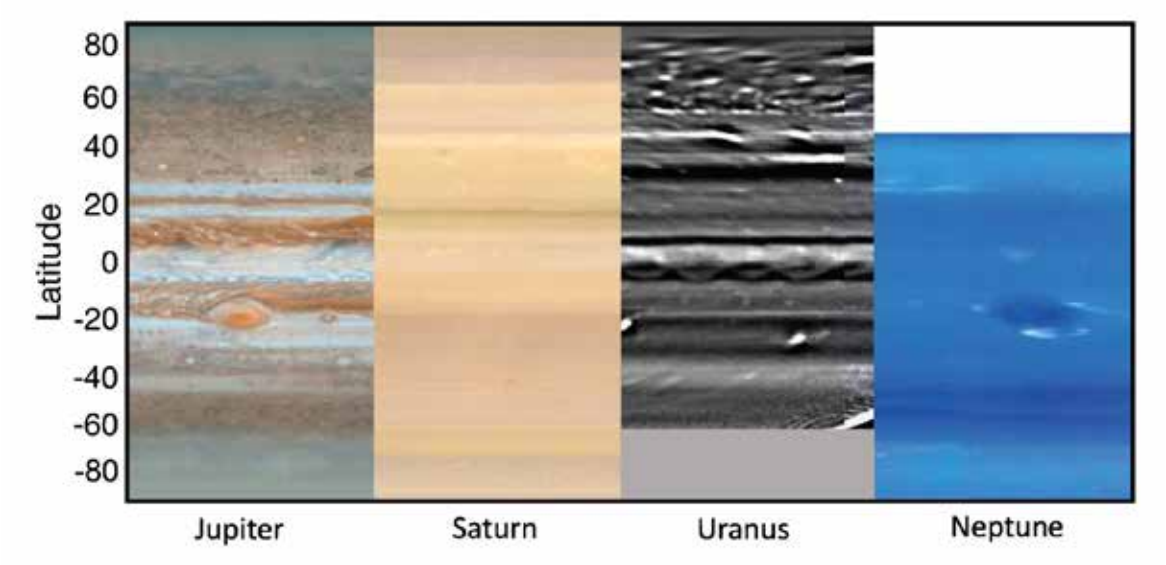

Fletcher et al. (2020, Space Sci. Rev.)

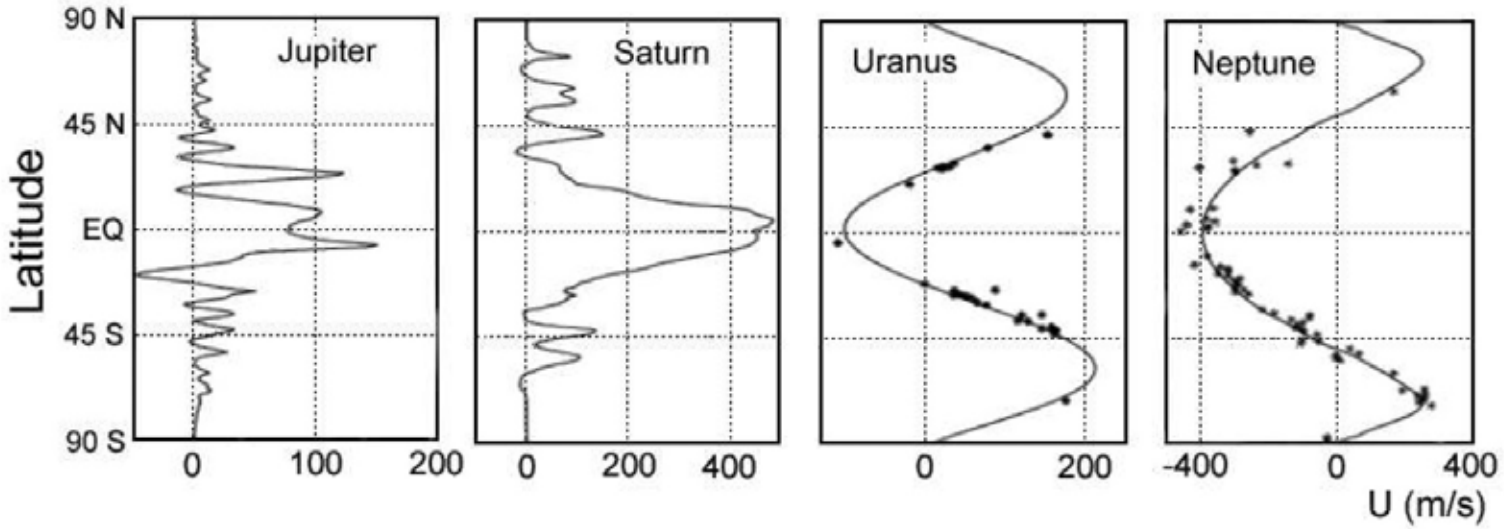

Sanchez-Lavega

Winds on Jupiter

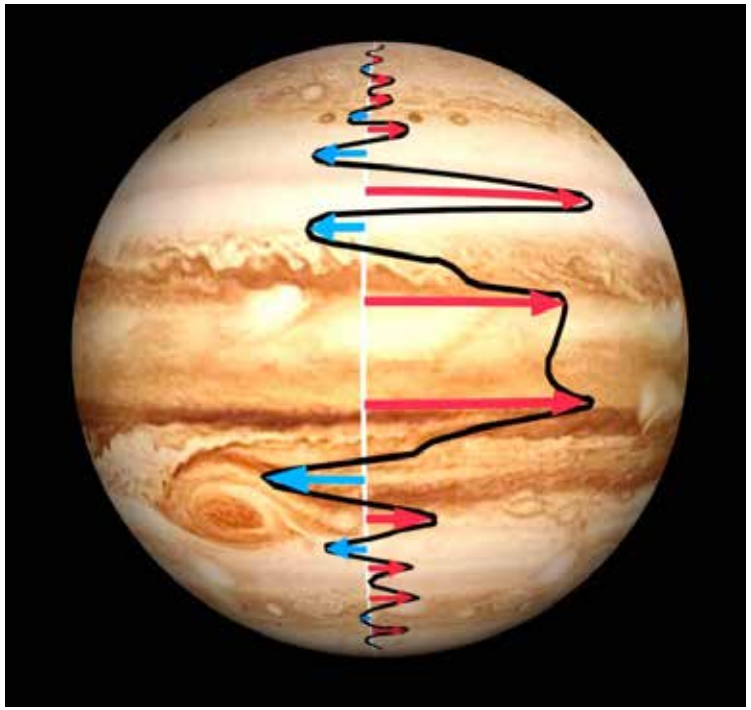

Zones :
- Reflective white bands of low temperatures, and elevated aerosol opacities
- Anti-cyclonic vorticity

Belts :
- Darker bands of warmer temperatures, and depleted aerosols
- Cyclonic vorticity

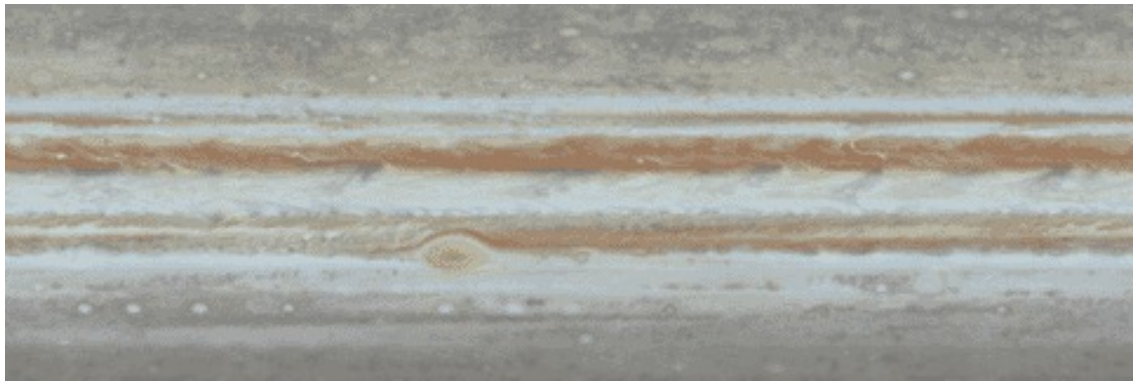

Cloud movie taken by Cassini spacecraft during its Jupiter flyby

Eddy momentum transport on Jupiter

Salyk et al. (2006)

Analysis of Cassini imaging data

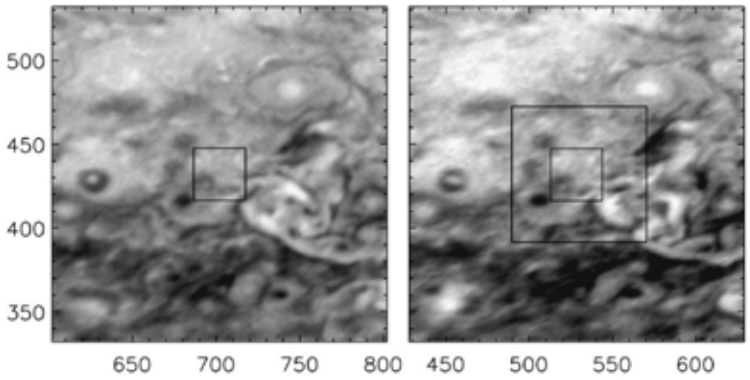

High positive correlation between eddy momentum flux, <u'v'>, and the variation of zonal velocity with latitude, du/dy, was found.

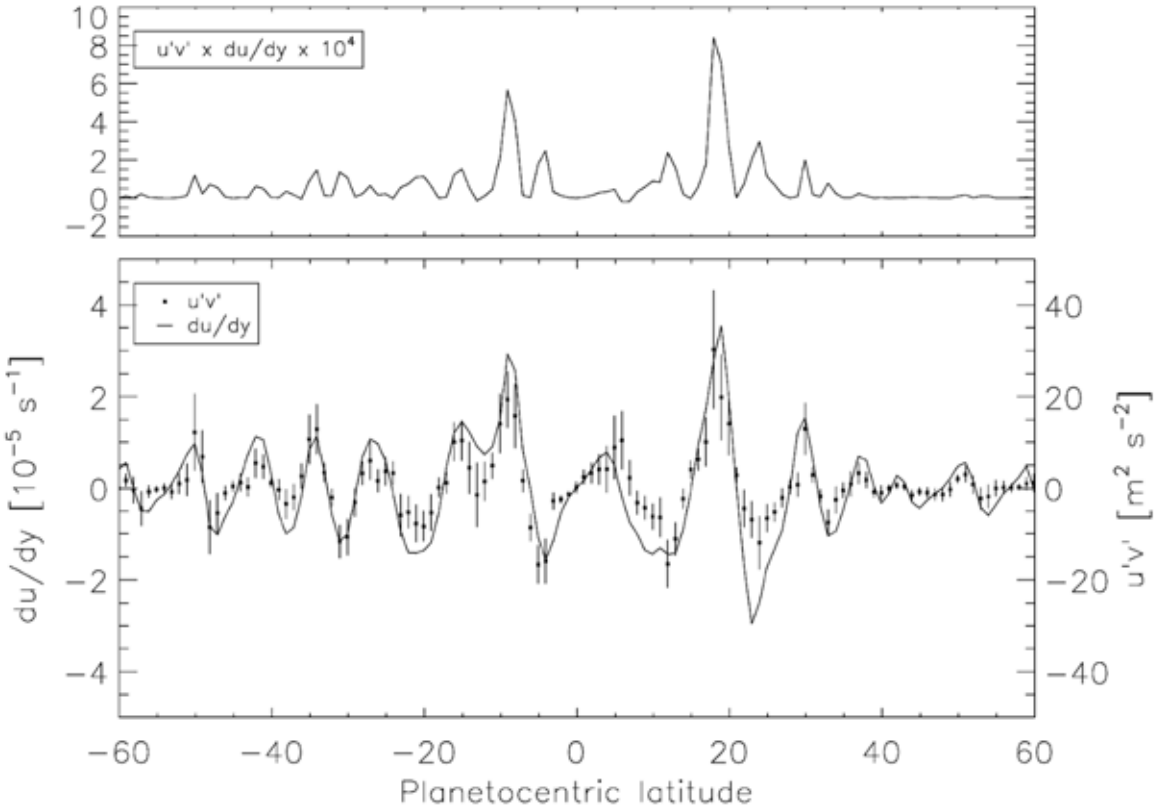

Thunderstorms on Jupiter

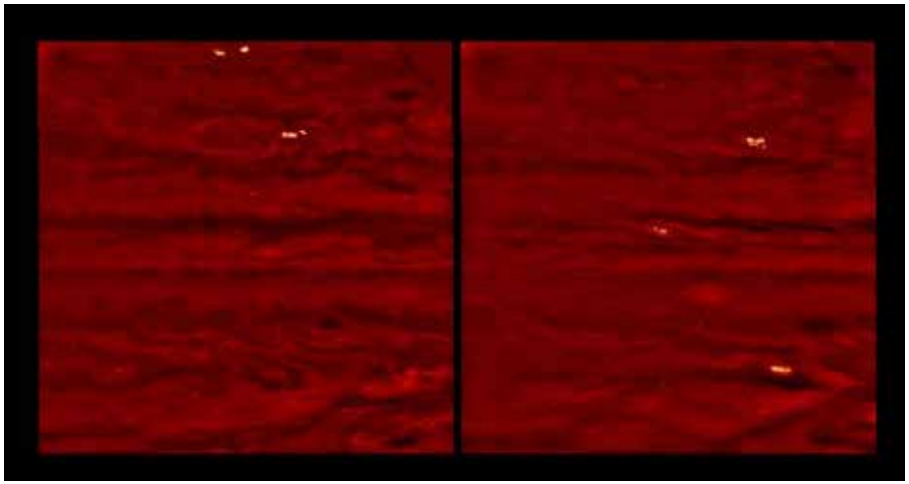

Lightning storms on the night side of Jupiter along with clouds dimly lit by moonlight from Io (taken by Galileo spacecraft)

On Jupiter, energy is transferred from the warm interior of the planet to the visible atmosphere to feed thunderstorms. Lightning occurs in the low-pressure regions.

Becker et al. (2020)

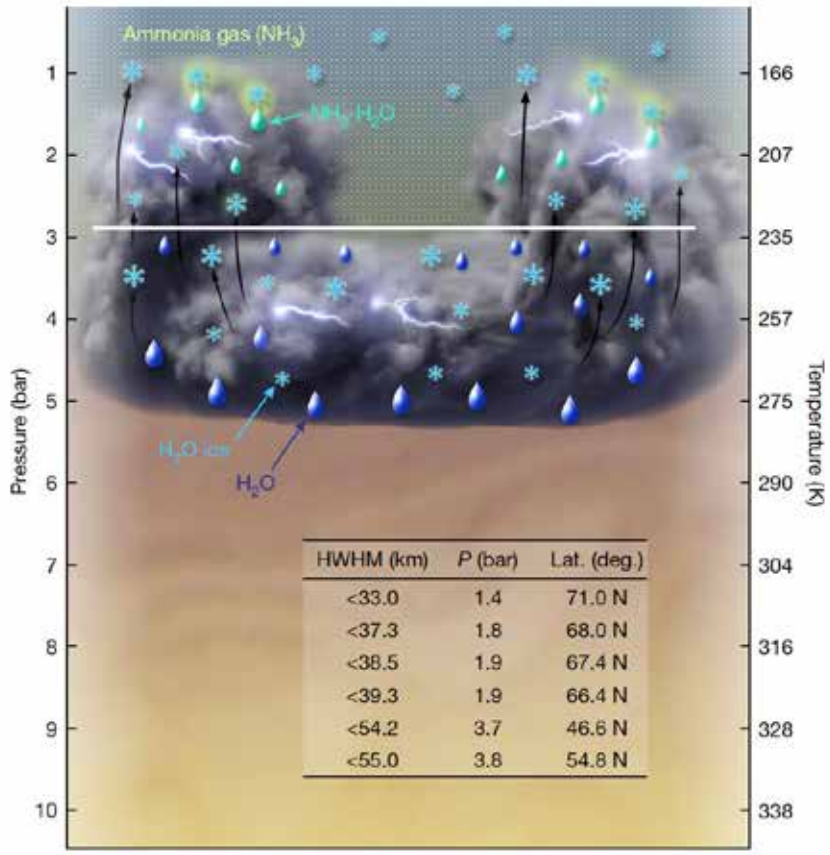

HWHM (km)	*P* (bar)	Lat. (deg.)
<33.0	1.4	71.0 N
<37.3	1.8	68.0 N
<38.5	1.9	67.4 N
<39.3	1.9	66.4 N
<54.2	3.7	46.6 N
<55.0	3.8	54.8 N

Fig. 3 | Conceptual illustration of lightning generation above and below the 3-bar level in Jupiter's atmosphere. Energetic updraughts (black arrows) loft water-ice particles to altitudes between 1.1 and 1.5 bar, where adsorption of ammonia gas onto ice particles melts the ice, creating falling liquid ammonia–water (NH_3–H_2O) particles (green drops). Charge separation occurs as the NH_3–H_2O particles collide with upward moving water-ice, followed by lightning. At pressures greater than about 3 bar, temperatures are above the limit for supercooled water (white line, about 233 K) and lightning is generated in pure water clouds. Inset, radial half-width at half-maximum (HWHM) intensity distances, estimated maximum depths of origin (*P*, pressure level) and latitudes (lat.) of observed SRU lightning flashes.

Superrotation on the gas giants

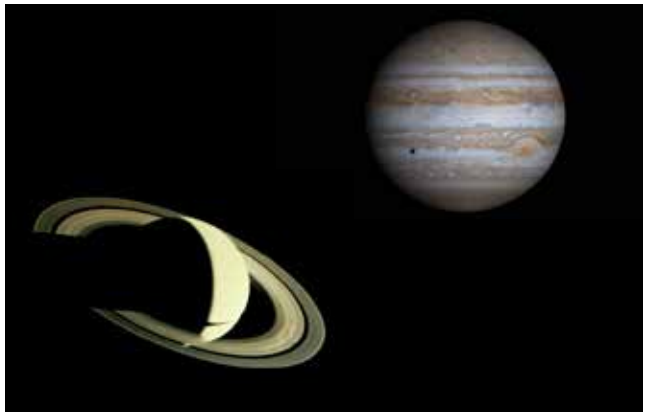

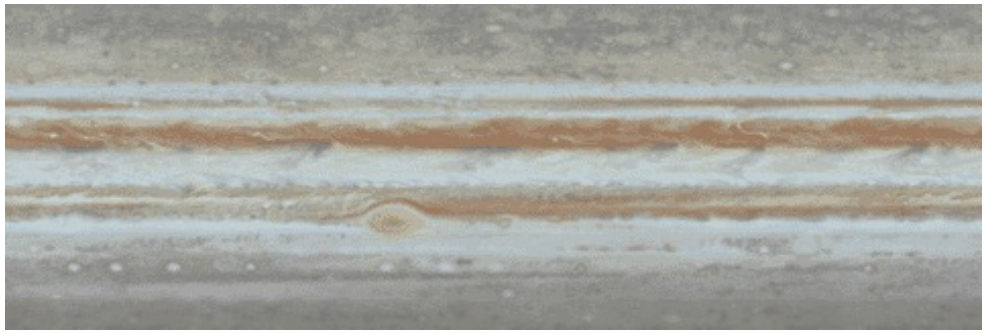

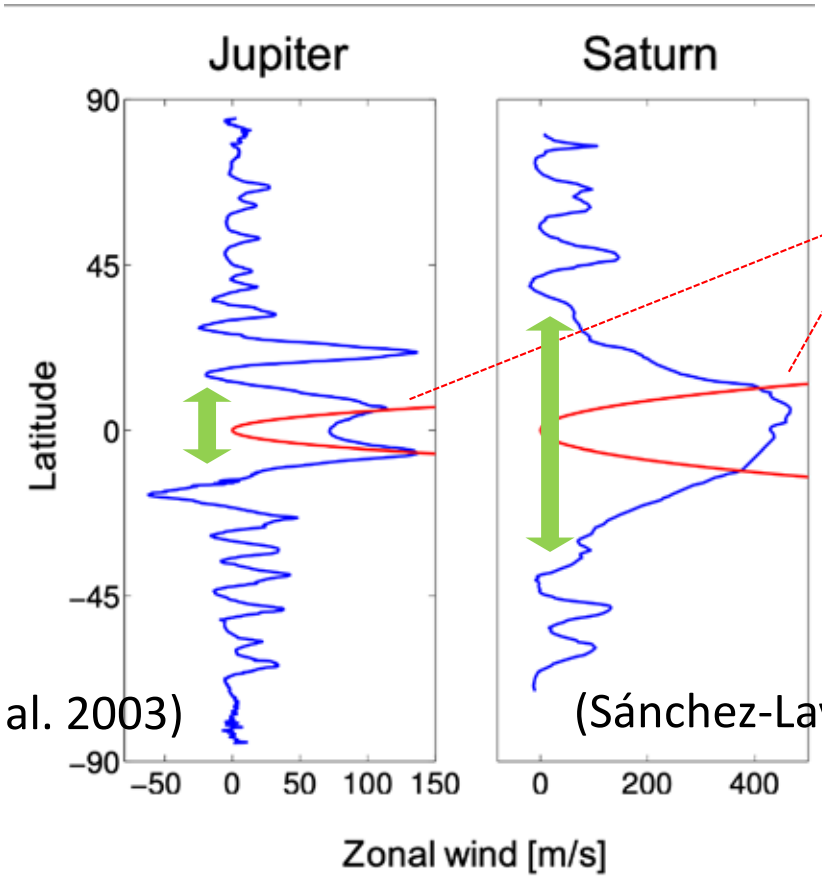

angular momentum conserving zonal velocity curve of a fluid parcel beginning at rest at the equator and moving poleward

(Porco et al. 2003)

(Sánchez-Lavega 2000)

Modeling Jupiter and Saturn's zonal flows

- Shallow models
  - The dynamics are shallow, such as on a terrestrial planet
  - The strong east-west flows can result from 2D geostrophic turbulence and/or baroclinic instability

- Deep models
  - the observed jets are the surface manifestation of convective columns originating from the hot interiors

Two-dimensional turbulence

- Small eddies tend to organize large eddies as time passes
- Turbulent energy cascade toward large scales (smaller wavenumber *k*)

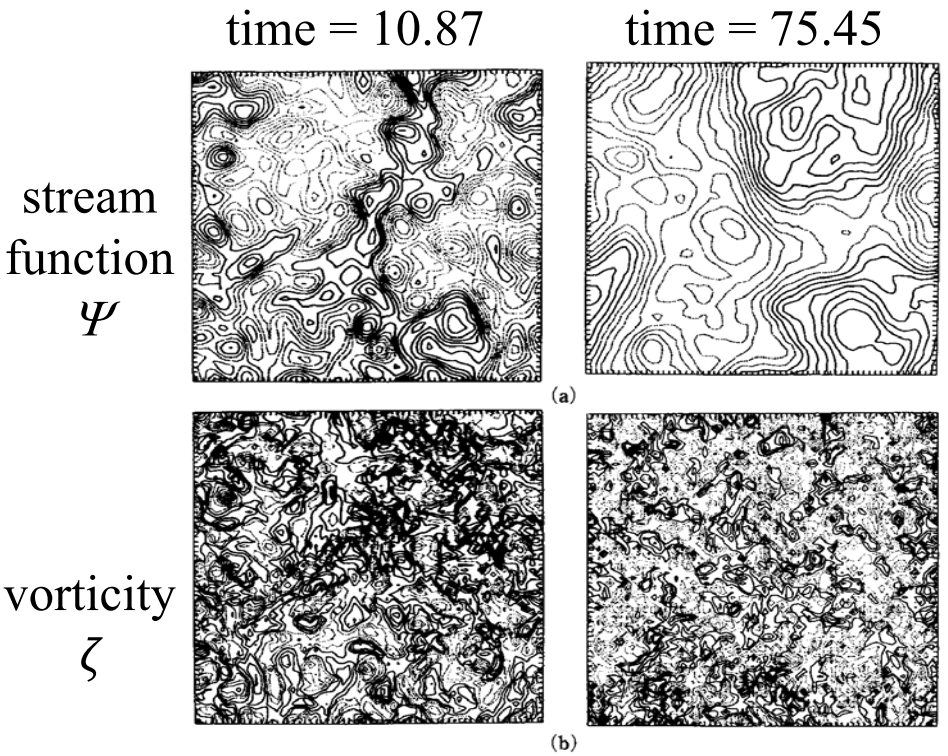

図 4.1 リリー（Lilly, 1969）の 2 次元乱流の数値実験の結果
左側の図が $t=10.87$，右側の図が $t=75.45$ での結果．(a)は流線関数，(b)は渦度の分布図．

Lilly (1969)

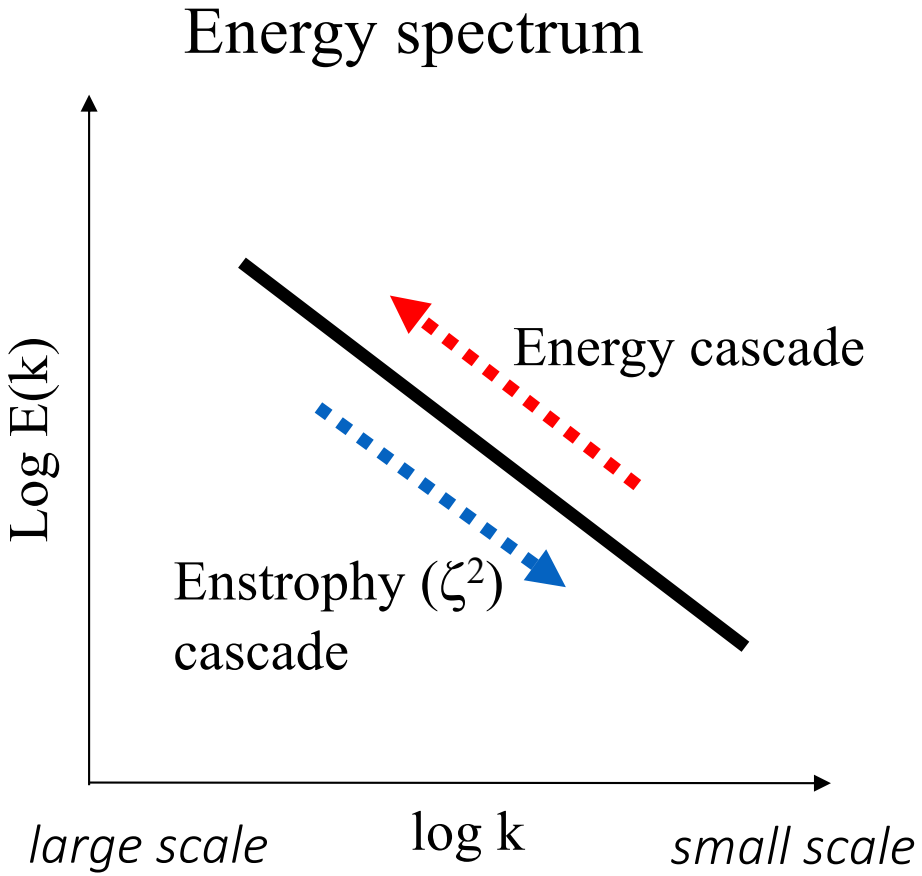

Rhines scale

- Vorticity equation

$$\left(\frac{\partial}{\partial t}+\vec{v}_g\cdot\nabla\right)(\zeta_g+f)=0$$

linearization

$$\frac{\partial\zeta}{\partial t}+u\frac{\partial\zeta}{\partial x}+v\frac{\partial\zeta}{\partial y}+\beta v=0$$

nonlinear term = origin of turbulence

linear term (beta effect) = origin of Rossby wave

$k^2 U^2 > \beta U$: turbulence

$k^2 U^2 < \beta U$: Rossby wave

β : df/dy

U : typical velocity

- Rhines scale

$$k_\beta=\sqrt{\frac{\beta}{U}}$$

Upward cascade of turbulence energy stops at smaller scales ($k < k_\beta$)

→ This transition scale corresponds to the width of the jets.

Shallow-water turbulence on the giant planets

- Forcing are given to the vorticity field as a small-scale, random process, or eddies are generated by baroclinic instability
- Inverse energy cascade generates multiple jets on the order of the Rhines scale
- The simulated equatorial flow is mostly retrograde

Scott & Polvani (2007)

Zonal velocity

Jupiter Saturn Uranus/Neptune

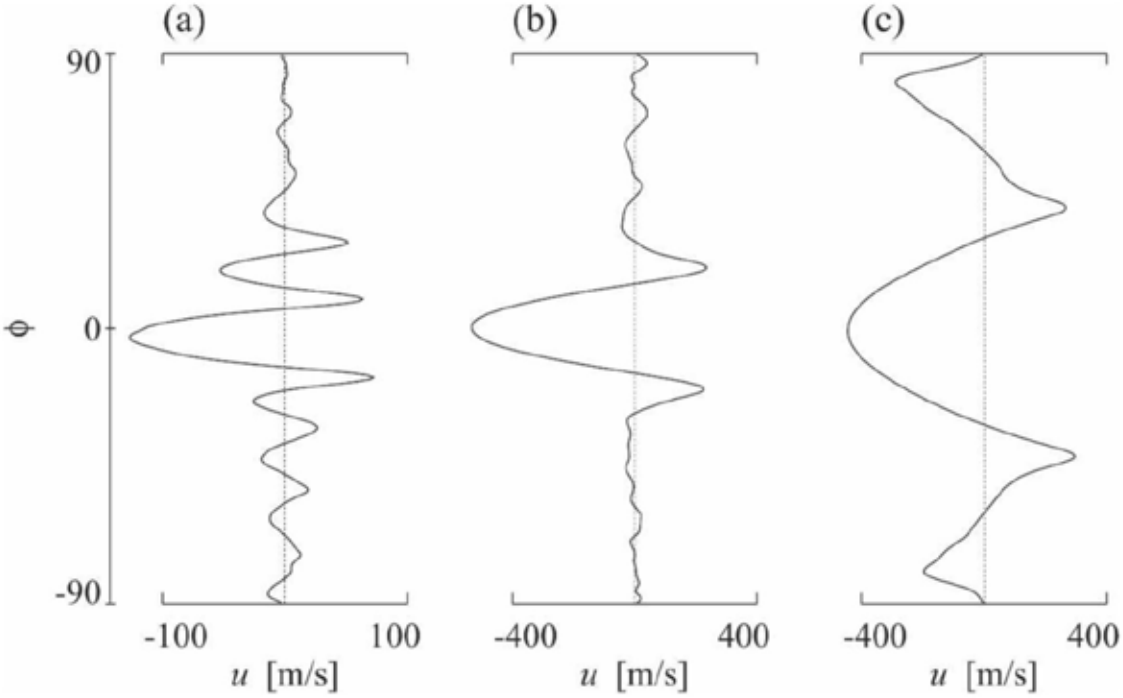

Vorticity field

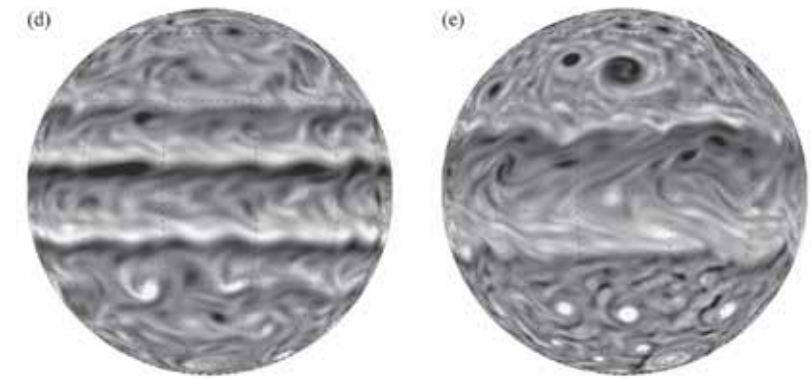

Jupiter (Ro=0.002) Saturn (Ro= 0.013)

Deep models: Taylor–Proudman theorem

- In a fluid that is steadily rotated, the fluid velocity will be uniform along any line parallel to the axis of rotation.

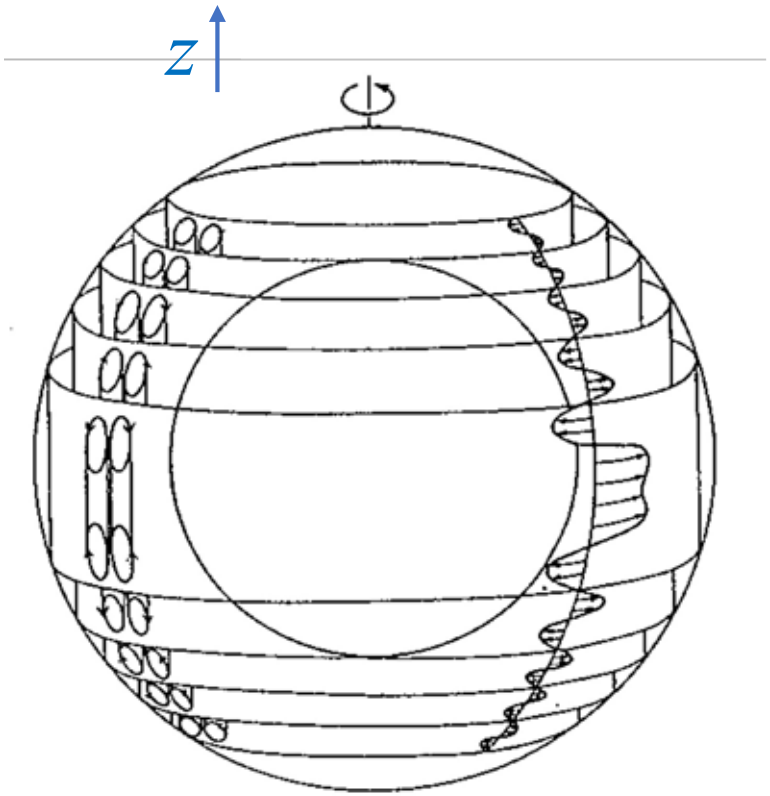

Busse (1994)

Momentum equation in rotational frame

$$\frac{d\vec{v}}{dt} + 2\vec{\Omega} \times \vec{v} + \frac{1}{\rho}\nabla p + \nabla\Phi = 0$$

Assuming non-compressivity and d/dt=0, the curl is applied to give

$$\vec{\Omega} \cdot \nabla\vec{v} = 0$$

Taking z-axis along the planet's rotational axis,

$$\frac{\partial\vec{v}}{\partial z} = 0$$

Thermal Rossby wave

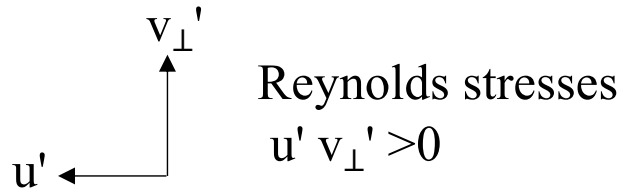

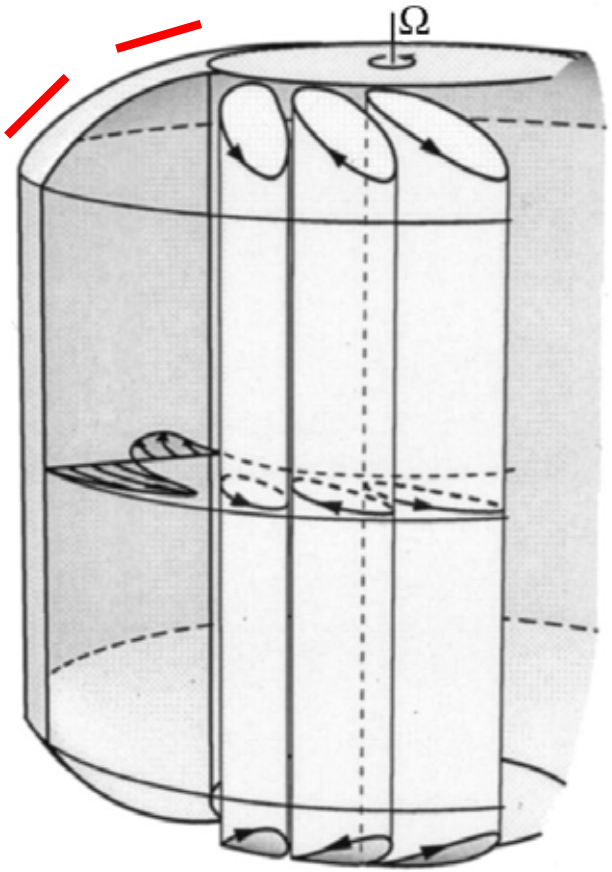

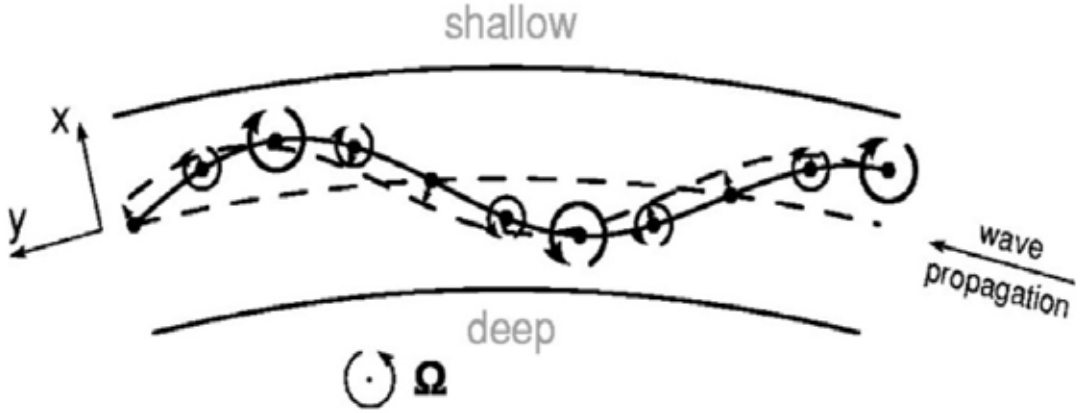

FIG. 2. The mechanism of propagation of a Rossby wave visualized in the equatorial plane of the rotating annulus: Fluid columns originally resting at the mid-surface acquire anticyclonic vorticity relative to the rotating system when they are displaced outwards towards the shallow region. Cyclonic vorticity is acquired by the displaced columns inwards. The action of the columnar motion on the neighboring fluid columns is such that an initial sinusoidal displacement propagates in the prograde direction.

Busse (2002)

The columns are tilted because the thermal Rossby wave has the tendency to propagate faster on the outside than on the inside. A prograde differential rotation on the outside with a retrograde one near the inner cylinder must thus be expected.

Quasi-geostrophic vorticity equation

$$\frac{\partial \zeta_g}{\partial t} = -\vec{v}_g \cdot \nabla(\zeta_g + f) + f_0 \frac{\partial \omega}{\partial p}$$

ω : Vertical velocity in *p*-coordinate

$$\zeta_g \equiv \frac{\partial v_g}{\partial x} - \frac{\partial u_g}{\partial y} = \frac{\nabla^2 \Phi'}{f_0}$$

: geostrophic vorticity

Vorticity changes with time through

- advection of absolute vorticity ($\varsigma_g + f$) by geostrophic wind ($\vec{v}_g$)
- vertical divergence (horizontal divergence)

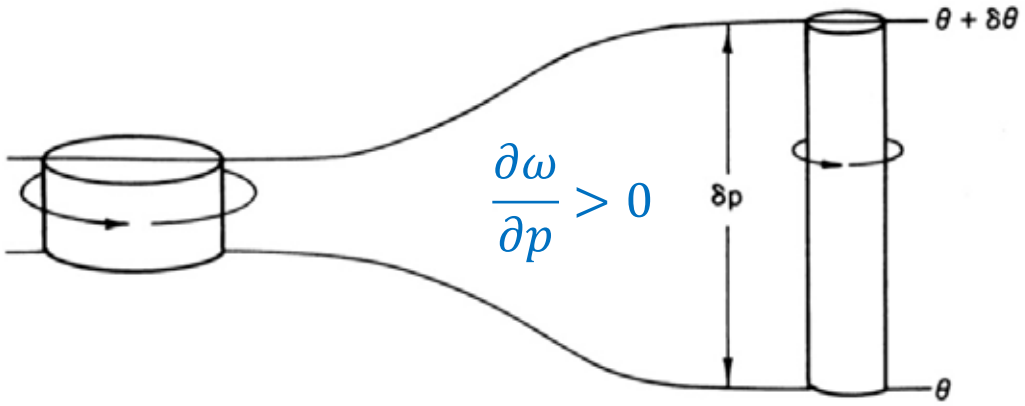

Holton (2004)

Fig. 4.7 A cylindrical column of air moving adiabatically, conserving potential vorticity.

Deep models

Observation

Model

Zonal velocity

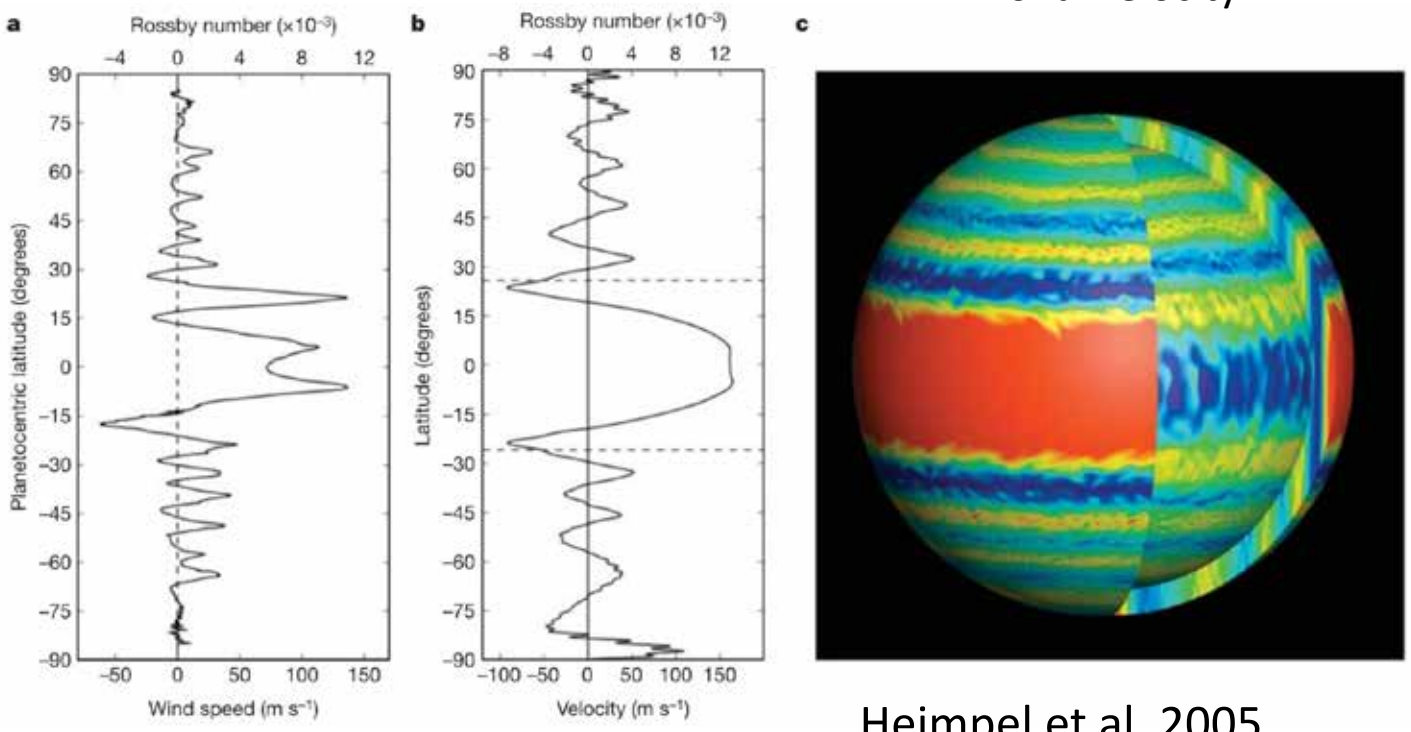

Heimpel et al. 2005

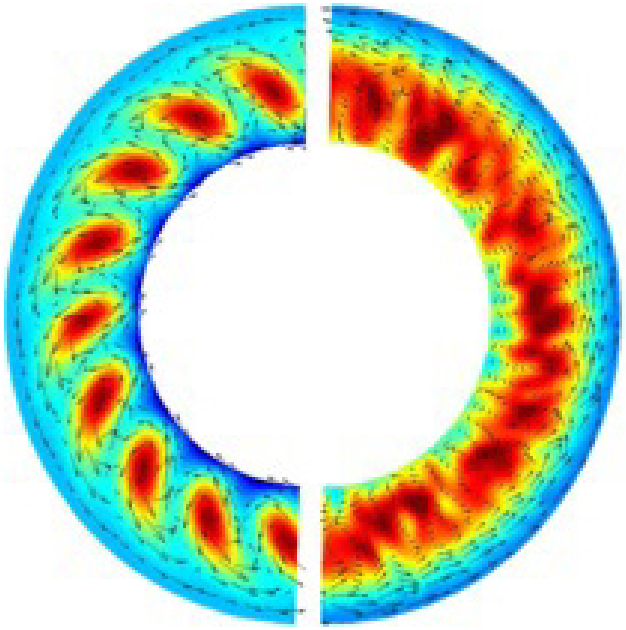

Showman et al. 2011

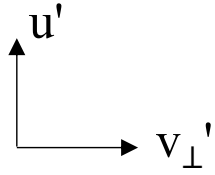

Reynolds stresses

$u' v_\perp' > 0$

Modeling of Jupiter

Schneider & Liu, 2009

baroclinic eddies generated by differential radiative heating are responsible for Jupiter's off-equatorial jets

zonal velocity

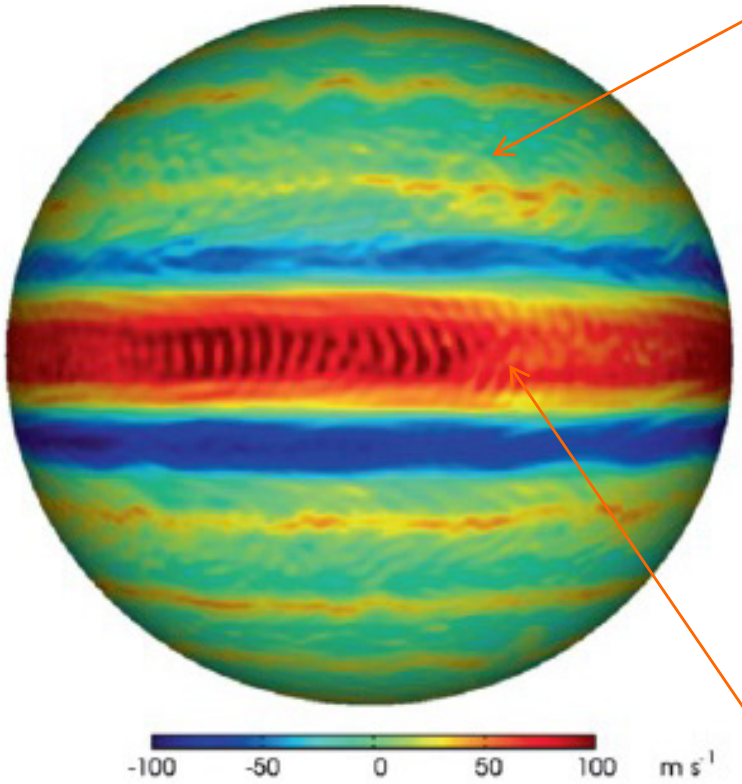

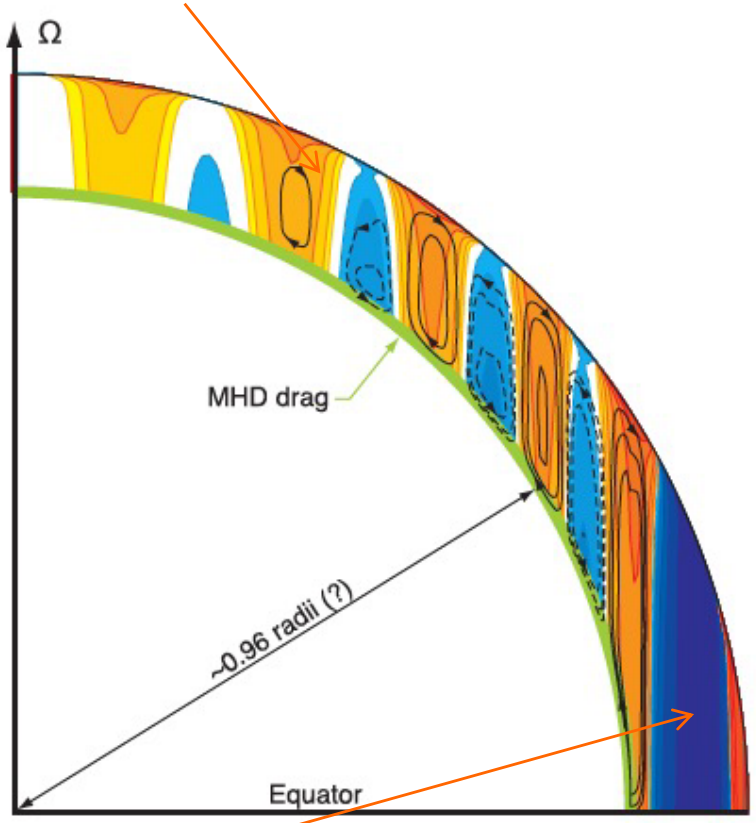

Rossby waves generated by intrinsic convective heat fluxes are responsible for the equatorial superrotation

Doppler tracking of Juno spacecraft

Less et al. (2018)

- The spacecraft acts as a test particle falling in the gravity field of the planet. Jupiter's gravity is inferred from range-rate measurements between a ground antenna and the spacecraft during perijove passes.
- The ground station transmits carrier signals, and the on-board translator lock the incoming carrier signals and retransmit them back to the ground. The range-rate (Doppler) observable is obtained by comparing the transmitted and received frequencies.
- Spherical harmonics representation of planetary gravity fields is determined by the density distribution inside the body.

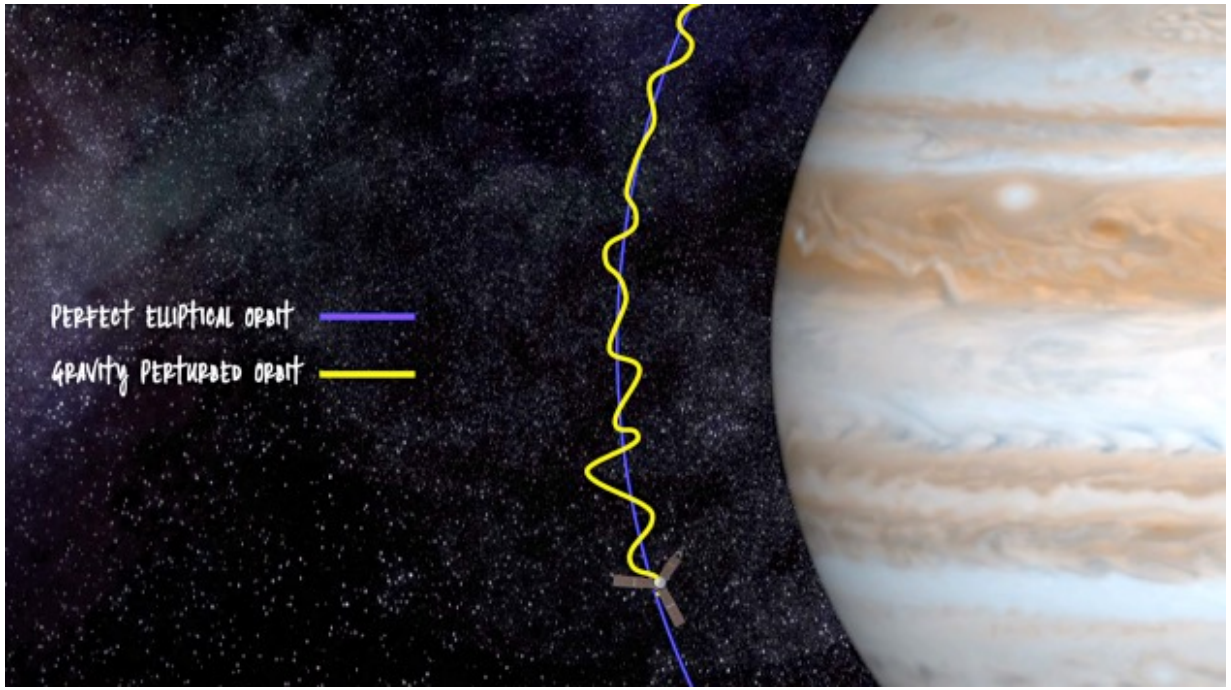

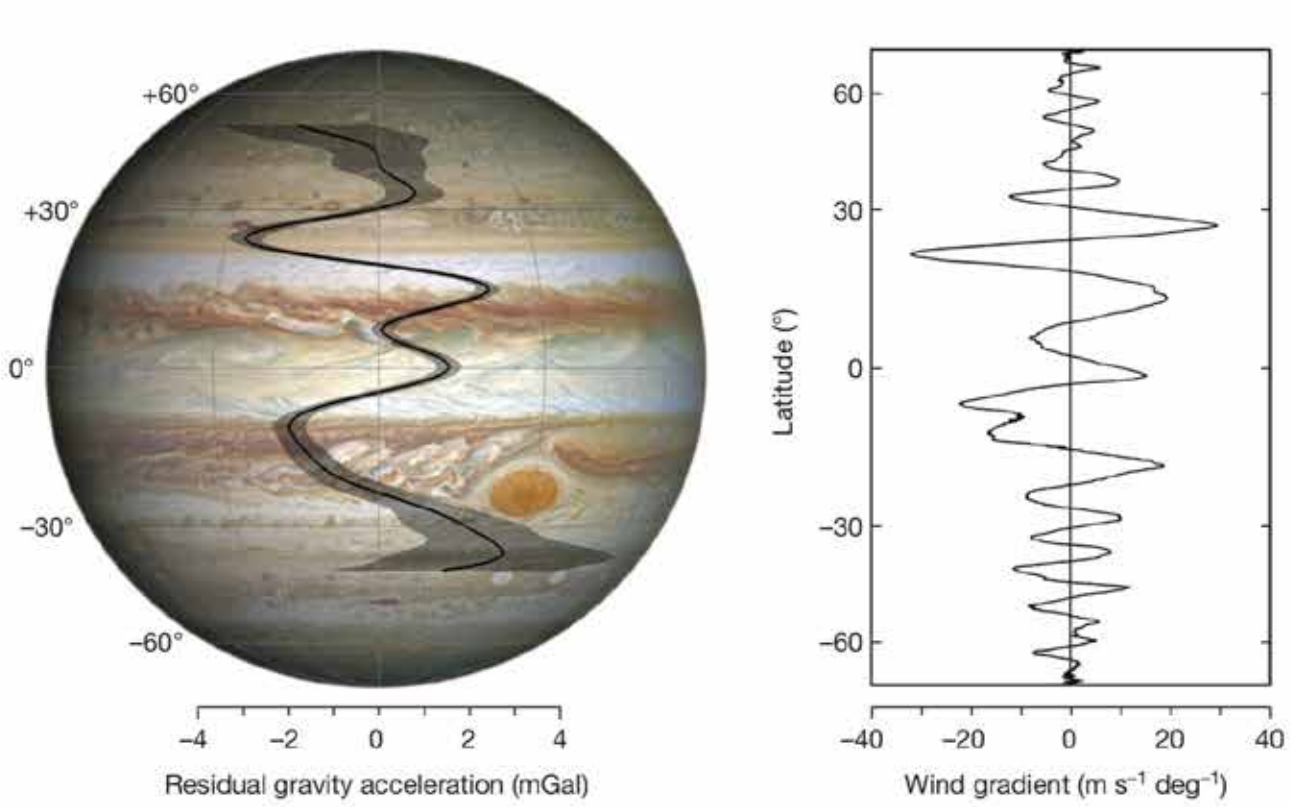

Figure 3 | Gravity disturbances due to atmospheric dynamics. a, An image of Jupiter taken by the Hubble Wide Field Camera in 2014 (https://en.wikipedia.org/wiki/Jupiter), showing the latitudinal dependence of residual gravity acceleration (in milligals, positive outwards) and associated 3σ uncertainty (shaded area) at a reference distance of 71,492 km, when the gravity from the even zonal harmonics J_2, J_4, J_6 and J_8 is removed. The residual gravity field, which is dominated by the dynamics of the flows, shows marked peaks correlated with the band structure. **b**, Latitudinal gradient of the measured wind profile. The largest (negative) peak of -3.4 ± 0.4 mGal (3σ) is found at a latitude of 24° N, where the latitudinal gradient of the wind speed reaches its largest value. The relation between the gravity disturbances and wind gradients is discussed in an accompanying paper[4].

Less et al. (2018)

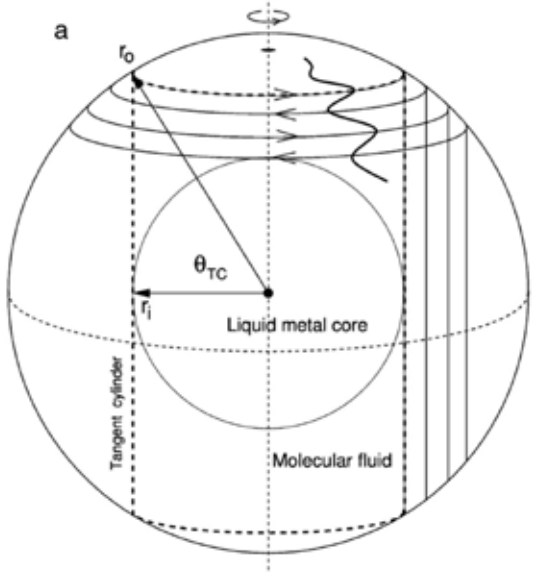

$$u(r,\theta) = u_{cyl}(s)Q(r) \tag{12}$$

where $u_{cyl}(s)$ is the cloud-level azimuthal wind projected downward along the direction of the axis of rotation, and $s = r\cos(\theta)$ is the distance from the axis of rotation. $Q(r)$ is the radial decay function we optimize, given by

$$Q(r)=(1-\alpha)\exp\left(\frac{r-a}{H(\theta)}\right)+\alpha\left[\frac{\tanh\left(-\frac{a-H(\theta)-r}{\Delta H}\right)+1}{\tanh\left(\frac{H(\theta)}{\Delta H}\right)+1}\right] \tag{13}$$

where a is the planetary radius, α is the contribution ratio between an exponential and a normalized hyperbolic tangent function and ΔH is the width of the hyperbolic tangent. We take a hierarchal approach using this profile at several levels of

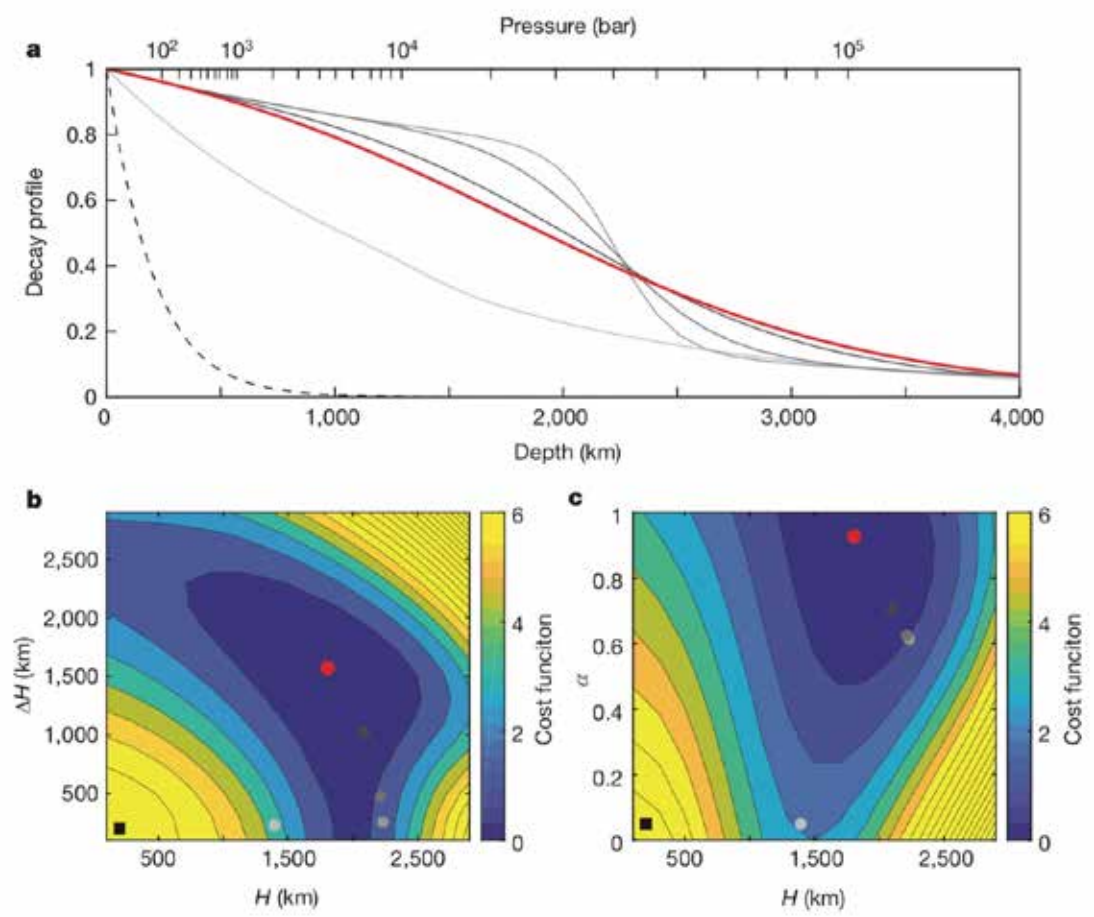

Kaspi et al. (2018)

The observed jet streams, as they appear at the cloud level, extend down to depths of thousands of kilometres beneath the cloud level, probably to the region of magnetic dissipation at a depth of about 3,000 kilometres

Difference between Jupiter and Saturn

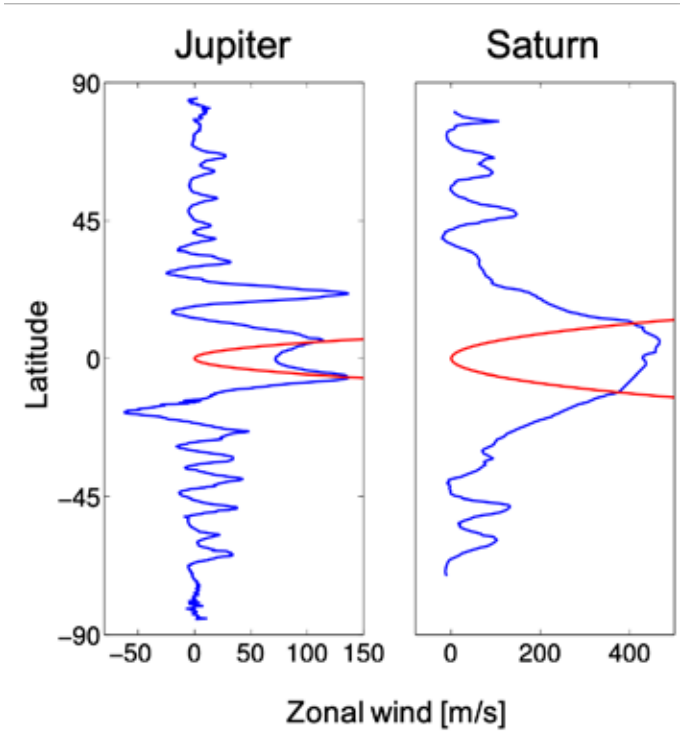

(Porco et al. 2003)

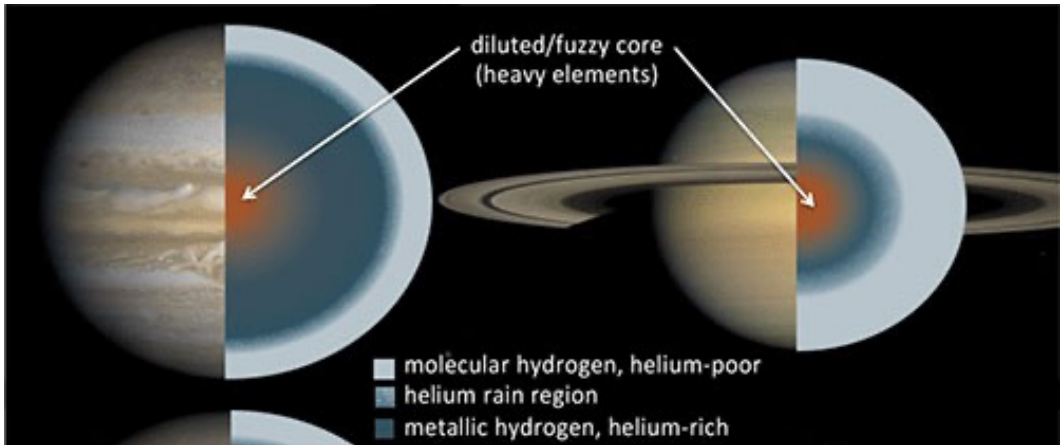

Helled (2019)

(Sánchez-Lavega 2000)

- According to gravity measurements by the Cassini spacecraft, Saturn's jets extend to about three times the depth of Jupiter's (Jupiter: 3000 km vs. Saturn: 9000 km). This is believed to correspond to depths where the atmosphere becomes conductive, causing Ohmic resistance.
- The latitudes at which equatorial super-rotation exists are <13° on Jupiter and <31° on Saturn. These transition latitudes correspond to where a line extended from the depth where conductivity occurs intersects the surface in the direction of the rotational axis.

Equatorial superrotation in the Sun

Rotation rates revealed by helioseismology

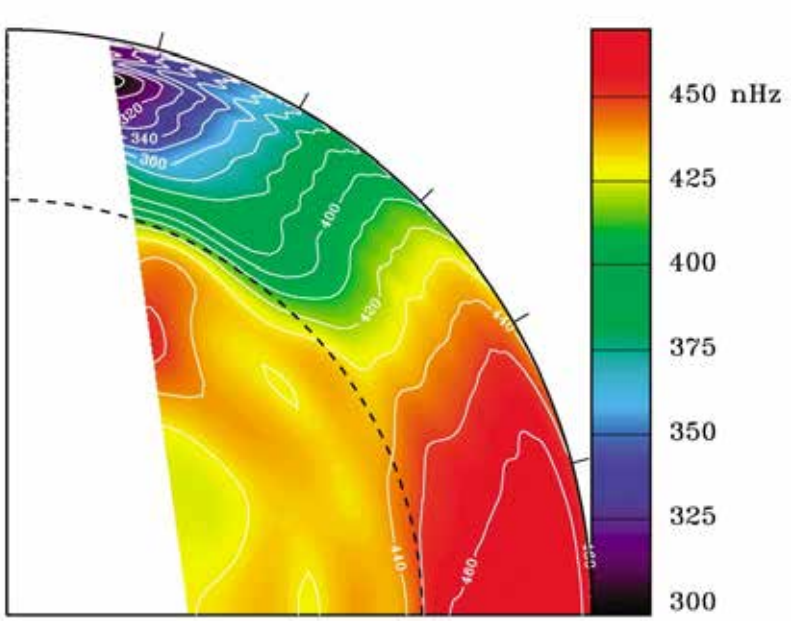

Rot. rate = 25 days on the equator

36 days near the poles

Numerical modeling (Miesch 2000)

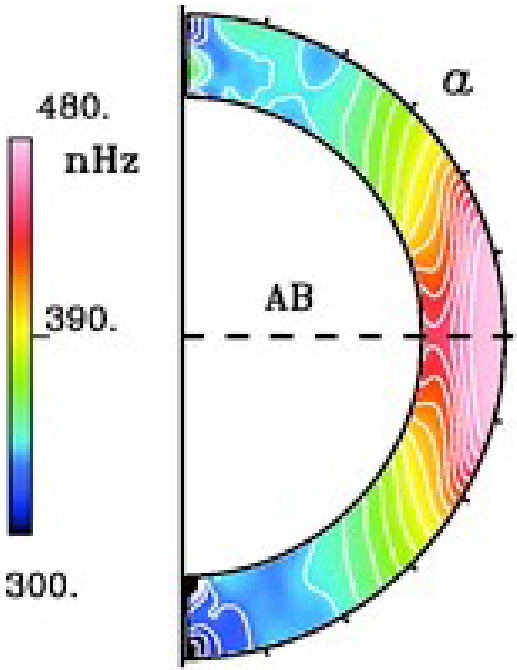

Vertical velocity at r = 0.95 $R_\odot$

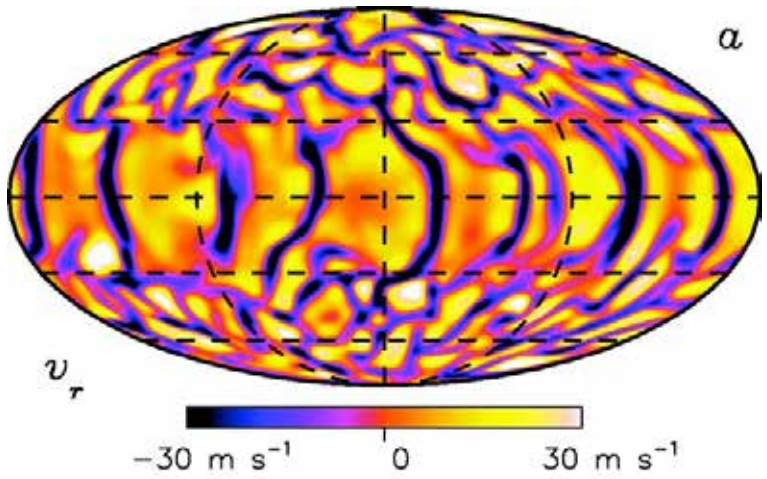

Equatorward angular momentum transport by slant convection ?